© 2014. Published by The Company of Biologists Ltd | Journal of Cell Science (2014) 127, 400–410 doi:10.1242/jcs.135079

RESEARCH ARTICLE

The RhoGAP ARHGAP19 controls cytokinesis and chromosome segregation in T lymphocytes

Muriel D. David*, Dominique Petit and Jacques Bertoglio*

ABSTRACT

Small GTP-binding proteins of the Rho family orchestrate the cytoskeleton remodelling events required for cell division. Guanine nucleotide exchange factors (GEFs) and GTPase-activating proteins (GAPs) promote cycling of Rho GTPases between the active GTP-bound and the inactive GDP-bound conformations. We report that ARHGAP19, a previously uncharacterised protein, is predominantly expressed in hematopoietic cells and has an essential role in the division of T lymphocytes. Overexpression of ARHGAP19 in lymphocytes delays cell elongation and cytokinesis. Conversely, silencing of *ARHGAP19* or expression of a GAP-deficient mutant induces precocious mitotic cell elongation and cleavage furrow ingression, as well as excessive blebbing. In relation to these phenotypes, we show that ARHGAP19 acts as a GAP for RhoA, and controls recruitment of citron and myosin II to the plasma membrane of mitotic lymphocytes as well as Rock2-mediated phosphorylation of vimentin, which is crucial to maintain the stiffness and shape of lymphocytes. In addition to its effects on cell shape, silencing of *ARHGAP19* in lymphocytes also impairs chromosome segregation.

KEY WORDS: Rho GTPases, Cytokinesis, Lymphocytes, Rock, Vimentin

INTRODUCTION

Cytokinesis, the process whereby one dividing cell splits its cytoplasm into two equal parts, involves drastic cell shape changes, especially for adherent cells that become spherical when entering mitosis and maintain contact with the extracellular matrix only through retraction fibres. For both adherent cells and cells dividing in suspension, such as lymphocytes, an ~1.5-fold elongation of the cell in anaphase precedes and accompanies ingression of the cleavage furrow that pinches off the cytoplasm at the cell equator. At later stages, again, morphological changes specific to adherent cells occur, in that daughter cells separated by an intercellular bridge re-adhere to the extracellular matrix, whereas cells dividing in suspension conserve their shape until the intercellular bridge is severed, hours later. Despite these differences in morphological changes during division of adherent and non-adherent cells, the molecular mechanisms regulating cytokinesis have been primarily studied using adherent cells (Kittler et al., 2007; Moffat et al., 2006; Neumann et al., 2006; Neumann et al., 2010) and little is known about how lymphocyte division is controlled.

In adherent cell cytokinesis, activation of the small GTPase RhoA by guanine nucleotide exchange factors (GEFs), such as Ect2, GEF-H1 and MyoGEF/PLEKHG6, increases cortical rigidity required for cell rounding in early mitosis and controls the actomyosin contractile ring during cleavage furrow ingression (Birkenfeld et al., 2007; Green et al., 2012; Jaffe and Hall, 2005; Kamijo et al., 2006; Maddox and Burridge, 2003; Tatsumoto et al., 1999; Wu et al., 2006). Although much attention has been given to the mechanisms by which Rho is activated during cytokinesis, it is still unclear how and when RhoA is inactivated. It remains to be determined whether GTPase-activating protein (GAP)-dependent downregulation of RhoA activity occurs throughout cytokinesis, to maintain an adequate level of active RhoA and/or to stimulate the RhoA GTPase flux (Miller et al., 2008), or much later in the division process. Moreover, only two GAP proteins that limit the activity of Rho family GTPases have been shown to be involved in cytokinesis. Experimental overexpression of p190A RhoGAP in adherent cells has been reported to decrease RhoA-dependent cleavage furrow ingression (Su et al., 2009), but the exact role of the endogenous protein has not been demonstrated. In adherent cells, RacGAP1/MgcRacGAP is paradoxically required for RhoA activation rather than for its inactivation (Loria et al., 2012) and was recently shown to act during anaphase to inhibit Rac1-dependent cell spreading and adhesion (Bastos et al., 2012). By contrast, the GAP activity of RacGAP1 is dispensable for cytokinesis in DT40 B lymphocytes (Yamada et al., 2006). Here, we describe a novel Rho GAP, ARHGAP19, which is predominantly expressed in cells of the hematopoietic lineage and is essential for cytokinesis in T lymphocytes.

RESULTS

Microarray analysis of Rho GTPase pathways in human leukaemia samples

During the course of experiments aimed at better understanding the role of Rho GTPases in hematopoietic cells, we analysed relative expression levels of 300 genes of the Rho GTPase pathways (GEFs, GAPs, effectors and Rho GTPases) in 100 samples of human T-cell acute lymphoblastic leukaemia whose transcriptome had previously been characterised (Soulier et al., 2005). Two-dimensional clustering brought together, on one hand, clinical samples displaying similar ‘Rho’ gene expression profiles and, on the other hand, genes of the Rho pathway whose expression levels co-varied across samples (Fig. 1A).

One of the gene clusters thus identified includes Ect2, RacGAP1, citron [three proteins with established roles in cytokinesis (Chalamalasetty et al., 2006)], Net1 [an oncogene that activates RhoA (Chan et al., 1996)], as well as ARHGAP11A and ARHGAP19, two proteins with unknown functions (Fig. 1B).

Inserm U749, Institut Gustave Roussy, 94805 Villejuif, France.

*Authors for correspondence (muriel.david@gustaveroussy.fr; jacques.bertoglio@gustaveroussy.fr)

Received 14 May 2013; Accepted 30 October 2013

Journal of Cell Science (2014) 127, 400–410 doi:10.1242/jcs.135079

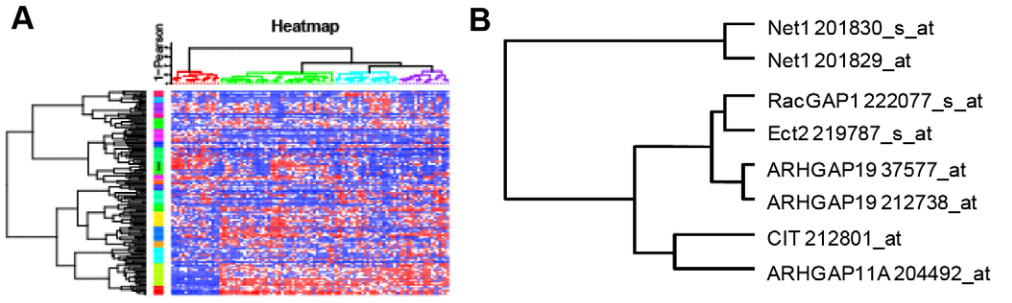

C

	Med Cor	GO biological process: Mitosis	GO biological process: Cytokinesis
DLG7	0.804	YES	
KIF2C	0.798	YES	
CCNB1	0.783	YES	
KIF18B	0.783	YES	
CENPA	0.782	YES	
KIF11	0.780	YES	
CDC2	0.779	YES	
KIF20A	0.779	YES	YES
CEP55	0.775	YES	YES
SPAG5	0.774	YES	
KIF14	0.772		
NEK2	0.771	YES	
CCNB2	0.768	YES	
KIF15	0.768	YES	
ASPM	0.767	YES	
CDKN3	0.764		
HMMR	0.763		
CCNA2	0.761	YES	
PBK	0.760	YES	
KIF23	0.758	YES	YES
NDC80	0.756	YES	
TOP2A	0.753	YES	
BUB1	0.752	YES	
PLK4	0.750	YES	YES
NCAPG	0.750	YES	
KIF4A	0.749	YES	YES
MELK	0.749		
NCAPH	0.749	YES	
CENPF	0.748	YES	
PTTG1	0.747	YES	
ESPL1	0.746	YES	YES
HJURP	0.745	YES	
PRC1	0.742	YES	YES
CENPE	0.741	YES	
CDC20	0.740	YES	
OIP5	0.740	YES	

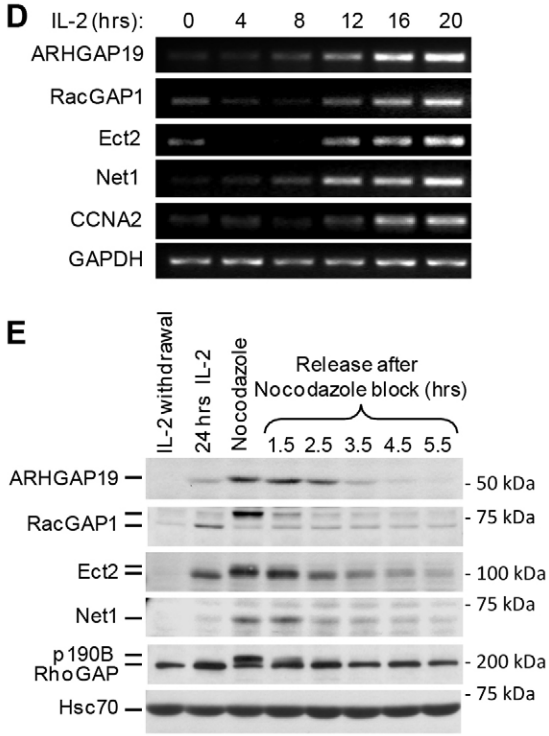

Fig. 1. Expression of the *ARHGAP19* gene co-varies with mitotic-related genes in human leukaemia samples and fluctuates through cell cycle progression in human T lymphocytes. (A) Unsupervised, two-dimensional clustering of levels of expression of 300 genes of the Rho pathways (vertical) in 100 samples of human T cell acute lymphoblastic leukaemia (horizontal). In the heatmap, gene expression levels are color-coded, with red and blue corresponding to higher and lower levels, respectively. (B) Part of the dendrogram corresponding to the gene cluster 'i' in A that illustrates distances between genes. (C) List of the top-correlated genes (i.e. correlation coefficient above 0.74) of the global transcriptome that co-vary with the cluster 'i' and, when stated in the GO database, mention of their involvement in mitosis and/or cytokinesis. (D,E) IL-2-dependent Kit225 cells were synchronised in G1 by factor deprivation, then stimulated to re-enter cell cycle by adding IL-2. Where indicated, cells were blocked in prometaphase using nocodazole, washed, and cultured for up to 5.5 hours. (D,E) RNA or proteins were purified from these cells and subjected to RT-PCR and western blotting, respectively. (D) Levels of mRNA encoding ARHGAP19, RacGAP1, Ect2 and Net1 co-varied with that of cyclin A2 (*CCNA2*), used here as an example of a gene induced during the S-phase. GAPDH was used as a loading control. (E) Western blot analyses showed maximal expression of the ARHGAP19, RacGAP1, Ect2 and Net1 proteins in mitosis. Such cell-cycle-dependent regulation of expression is not a hallmark for all Rho pathway components, however, in that the level of the p190B RhoGAP protein remains constant during T lymphocyte cell-cycle progression. Hsc70 was used as a loading control.

Among the 36 genes of the global transcriptome that co-vary the most with this cluster, 32 code for proteins whose role in cell division is already established (Fig. 1C). This enrichment in genes coding for proteins involved in cell division suggested that ARHGAP19 and ARHGAP11A might, like Ect2, RacGAP1 and citron, participate in the control of mitosis or cytokinesis. We tested this hypothesis, and focused our study on ARHGAP19 because, with the noticeable exception of germ cells, it is expressed predominantly in cells of hematopoietic origin (supplementary material Fig. S1).

ARHGAP19 expression levels fluctuate in T lymphocytes during the cell cycle

Variations in ARHGAP19 levels during progression through IL-2-induced cell cycling of Kit225 T lymphocytes were monitored by RT-PCR. mRNA encoding ARHGAP19, RacGAP1, Ect2 and

Journal of Cell Science (2014) 127, 400–410 doi:10.1242/jcs.135079

Net1 were induced together with mRNA encoding cyclin A2, during the S-phase of cell cycle (Fig. 1D) (Seguin et al., 2009). Similar to RacGAP1, Ect2 and Net1, ARHGAP19 protein was undetectable in G1, appeared during the S–G2 phases, peaked at mitosis, and then dropped at the beginning of the next cell cycle (Fig. 1E). The correlative variations in expression of ARHGAP19, Ect2 and RacGAP1, with maximal levels during mitosis, suggested that these proteins operate sequentially or in concert to regulate aspects of a shared cell function.

ARHGAP19 shuttles between the nucleus, cytoplasm and cell cortex

We next investigated localisation of ARHGAP19 during the cell cycle. Consistent with our finding that ARHGAP19 expression is regulated during the cell cycle, many cells in interphase were not stained by the anti-ARHGAP19 antibody. When present, staining was primarily detected in the cell nuclei (Fig. 2A). Subcellular localisation of ARHGAP19 varied during mitosis (Fig. 2B). In prophase and metaphase, ARHGAP19 was dispersed in the cytoplasm. In early anaphase, ARHGAP19 was enriched along the cell periphery, whereas at later stages and until the end of cell division ARHGAP19 was concentrated at the cortical region of the ingressing cleavage furrow.

The level and activity of ARHGAP19 affect the timing of cell elongation and cleavage furrow formation, and impact chromosome segregation

To investigate the role of ARHGAP19 in lymphocyte division, we engineered populations of Kit225 lymphocytes in which expression of ARHGAP19 was either increased through transfection with plasmids allowing doxycyclin-induced expression of the GFP-ARHGAP19 fusion protein, or silenced through transfection with shRNA constructs (Fig. 3A). Time-lapse microscopy experiments revealed that manipulation of ARHGAP19 levels had an impact on two aspects of cell division: the time of cell shape changes (cell elongation and cleavage furrow formation) and chromosome segregation (Fig. 3B–G and supplementary material Movies 1–4).

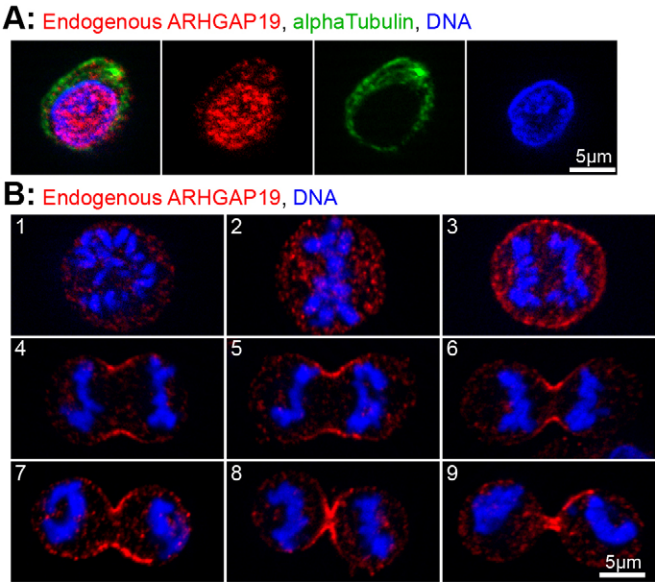

Fig. 2. Localisation of endogenous ARHGAP19 in interphase and throughout cell division. (A) Untransfected Kit225 lymphocytes were fixed with paraformaldehyde and labelled for α-tubulin (green), DNA (blue) and ARHGAP19 (red) using our home-made anti-ARHGAP19 antibody. Shown is a cell in interphase that stained positive for ARHGAP19. Of note, similar results were also obtained using the anti-ARHGAP19 from GeneTex, and the specificity of both these antibodies for ARHGAP19 was demonstrated by their inability to stain ARHGAP19-depleted lymphocytes (not shown). (B) Untransfected Kit225 lymphocytes were fixed with trichloroacetic acid and labelled for ARHGAP19 (red) and DNA (blue). In prophase (1) and metaphase (2), ARHGAP19 is dispersed in the cytoplasm. After anaphase onset, ARHGAP19 is recruited at the cell periphery (3). During cleavage furrow ingression and until the end of telophase (4–9), ARHGAP19 concentrates at the equatorial cortex.

Silencing or overexpression of *ARHGAP19* induced opposite effects on morphological changes and mitotic blebbing. In control cells, elongation and furrow ingression occurred 3 and 4 minutes after anaphase onset, respectively. In cells overexpressing ARHGAP19, these two events were postponed to 7 and 8 minutes after anaphase onset, respectively, and mitotic blebs were abolished. Despite the significant delays in cell elongation and cleavage furrow ingression, most of these cells successfully completed mitosis. By contrast, ARHGAP19-depleted mitotic lymphocytes displayed signs of cortical hyper-contractility, such as excessive blebbing. About half of these cells started elongating earlier than control cells, on average 2 minutes before anaphase onset. Cleavage furrow ingression also occurred earlier than in control cells, only 2 minutes after anaphase onset. Of note, about 44% of the ARHGAP19-deficient lymphocytes could not be taken into account in these quantitative analyses of time of cell elongation or of cleavage furrow ingression, because of the occurrence of chromosome mis-segregation events that made difficult determination of the exact time of anaphase onset. Because severe defects in chromosome segregation were often preceded by extensive cell shape remodelling in early mitosis, the morphological phenotypes induced by depletion of ARHGAP19 are probably underestimated in the quantifications shown in Fig. 3F,G.

Silencing of *ARHGAP19* affected chromosome segregation in 43.6% of the ARHGAP19-deficient lymphocytes: at the time of cleavage furrow contraction, chromosomes had not fully segregated away from the furrow area, and lagging DNA persisted in the intercellular bridge (Fig. 3D, middle and bottom panels). Occasionally, cytokinesis reversion occurred [possibly because of lagging DNA-induced activation of the NoCut pathway (Mendoza et al., 2009; Norden et al., 2006; Steigemann et al., 2009)], leading to cell binucleation. Similar phenotypes were obtained when *ARHGAP19* was silenced in Jurkat lymphocytes (supplementary material Fig. S2).

Because manipulation of ARHGAP19 levels impacted both morphological changes and chromosome segregation, the question arose as to whether these two aspects were mechanistically linked or instead could occur independently. To ascertain that, indeed, ARHGAP19 regulates cell shape in early mitosis, lymphocytes were treated with nocodazole, which blocks mitosis progression at the prometaphase stage. Anti-phospho-H3 staining was performed to ensure that experimental variations in ARHGAP19 levels did not affect the spindle assembly checkpoint and that lymphocytes from all the nocodazole-treated populations were properly arrested in mitosis (Fig. 4A). More than 60% of the ARHGAP19-depleted lymphocytes became elongated and adopted improbable shapes. By contrast, 90% of the ARHGAP19-overexpressing lymphocytes remained round (Fig. 4A,B). Control cells showed an intermediate behaviour. This result confirmed that manipulation of ARHGAP19 levels impacts cell shape during early mitosis, and indicated that this aspect of the phenotype does not rely on microtubule dynamics or chromosome segregation. Demonstrating that chromosome mis-segregation in ARHGAP19-depleted lymphocytes could occur

Journal of Cell Science (2014) 127, 400–410 doi:10.1242/jcs.135079

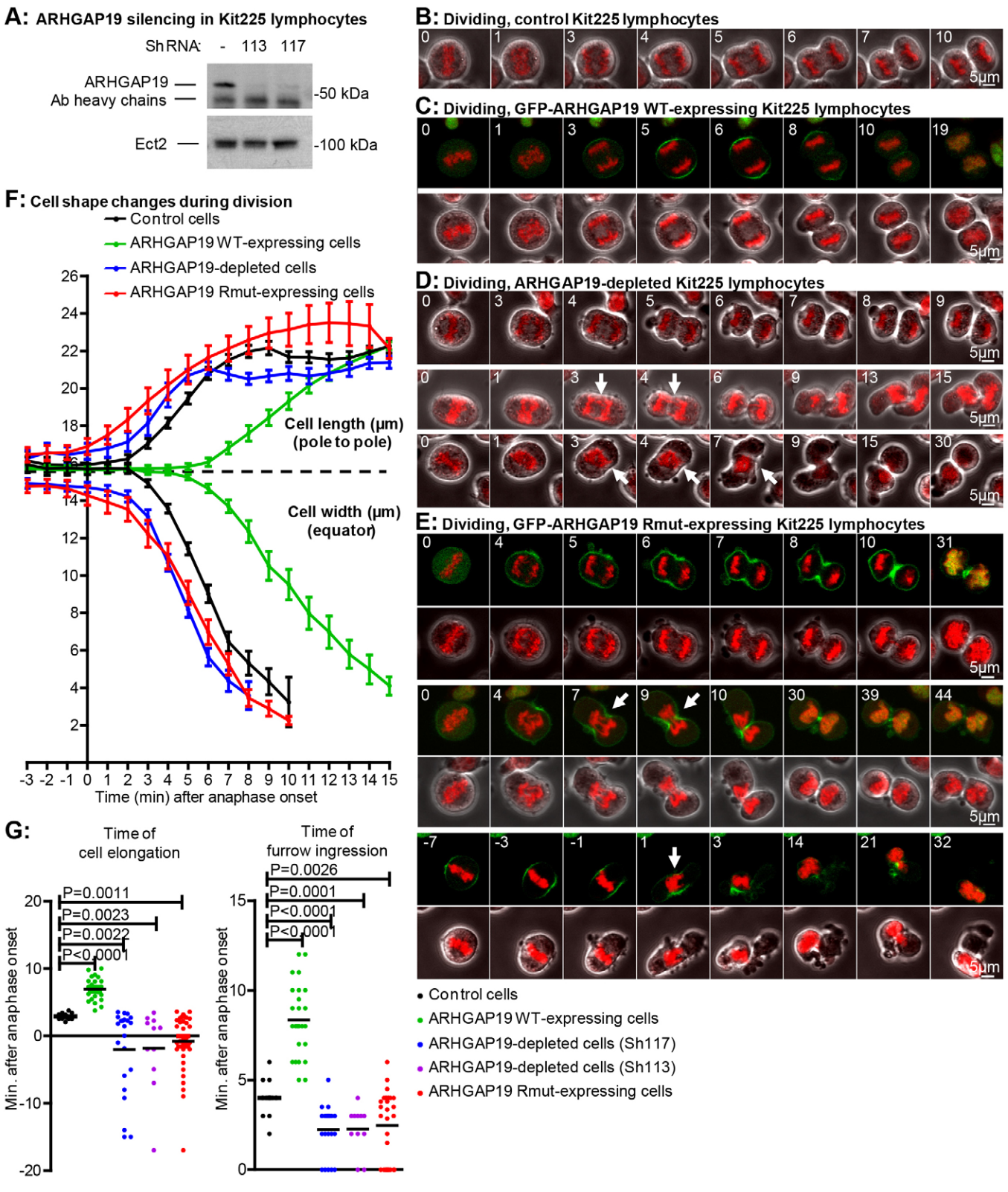

Fig. 3. See next page for legend.

independently of earlier abnormalities in morphological changes proved more challenging. Although extensive cell shape remodelling in early mitosis was often followed by severe defects in chromosome segregation, the extents of these two aspects of the phenotypes were not always correlated. For example, despite the fact that the ARHGAP19-depleted lymphocyte shown in the middle panel of Fig. 3D elongated long before anaphase onset, chromosome plates efficiently segregated toward the cell

Journal of Cell Science

Journal of Cell Science (2014) 127, 400–410 doi:10.1242/jcs.135079

Fig. 3. Manipulation of ARHGAP19 levels impacts timing of cell elongation and cleavage furrow formation, as well as mitotic blebbing and chromosome segregation in human lymphocytes. (A) Kit225 lymphocytes transfected or not (-) with the ShRNA 113 or 117 were synchronised in prometaphase using nocodazole. Efficiency of ARHGAP19 depletion was confirmed through immunoprecipitation followed by western blotting. Evaluation of Ect2 expression was used as an input control. (B–E) Mitosis progression of 18 control Kit225 lymphocytes (B), 25 lymphocytes expressing WT GFP-ARHGAP19 Kit225 (C), 34 ARHGAP19-depleted Kit225 lymphocytes (D) and 35 Kit225 cells expressing Rmut GFP-ARHGAP19 (E) was followed by time-lapse microscopy. Selected frames of representative videos are displayed. The red colour corresponds to fluorescence emitted by the DNA labelling, Syto 59 dye. In C and E, the green colour corresponds to the GFP signal. Time '0 min' was set on the last frame displaying the cell at the metaphase stage. (C) 100% of the cells expressing WT GFP-ARHGAP19 showed significant delays in cell elongation and time of cleavage furrow formation compared with control cells. (D) The top panel illustrates the 56.4% of the ARHGAP19-depleted cells that performed a rather normal mitosis, although excessive blebbing can be noted. The middle and bottom panels illustrate the defects observed in the remaining 43.6% of these cells, including precocious cell elongation and cleavage furrow ingression occurring before effective segregation of the chromosomes away from the furrow area. White arrows indicate lagging DNA. (E) 34.3% of the Rmut GFP-ARHGAP19 cells performed normal division, although excessive blebbing can be noted (top panel). The middle and bottom panels illustrate the remaining 65.7% of these cells for which mitosis is severely perturbed, with phenotypic abnormalities reminiscent of those observed in ARHGAP19-depleted cells. White arrows indicate lagging DNA. This highlights the role of the GAP domain of ARHGAP19 in cell division control, and suggests that Rmut GFP-ARHGAP19 acts as a dominant negative. See also supplementary material Movies 1–4. (F,G) Quantitative analyses (mean ± s.e.m.) of the movies. (F) Cell length and cell width at the equator or furrow were measured every minute during mitosis progression. (G) Time of cell elongation or cleavage furrow ingression were defined as the periods separating the last frame showing cells in metaphase and the first frame showing cells with an elongated morphology (length/width >2 μm), or the first frame showing a furrow, respectively. Unpaired, two-tailed *t*-tests were performed using GraphPad software to determine whether means significantly differed between cell populations. Of note, the ARHGAP19-deficient lymphocytes in which chromosome mis-segregation was so pronounced that the exact time of anaphase onset was difficult to determine were not included in these quantifications.

poles (although some lagging DNA was detectable). By contrast, the ARHGAP19-depleted lymphocyte shown in the bottom panel of Fig. 3D elongated only after anaphase onset, and nevertheless displayed much worse defects in chromosome segregation. Thus, each of the two aspects of the phenotype is probably a direct consequence of manipulation of ARHGAP19 levels, and can occur independently of each other.

To investigate whether the functions of ARHGAP19 depended on its putative GAP activity, we mutated the predicted catalytic arginine residue (R143) of the GAP domain. 34.3% of GFP-ARHGAP19 Rmut-expressing Kit225 cells divided without noticeable defects (top panels of Fig. 3E). The remaining 65.7% of these cells displayed mitotic abnormalities. Indeed, cells often became ovoid as soon as the metaphase stage and defective chromosome segregation at the time of cleavage furrow ingression was frequently observed (middle and bottom panels of Fig. 3E). Expression of the Rmut form of GFP-ARHGAP19 also induced major blebbing and/or additional cleavage furrows, and daughter cells often wiggled extensively for several hours following cytokinesis. Thus, expression of the Rmut form of GFP-ARHGAP19 did not reproduce the effects triggered by the WT, which demonstrates that the phenotypes induced by the WT rely on integrity of the GAP domain. Instead, the Rmut form triggered opposite effects, which were reminiscent of those observed in the two independent populations of shRNA-transfected lymphocytes, suggesting that it acts as a dominant negative.

ARHGAP19 displays GAP activity on RhoA, but not Rac1 or CDC42

That the mitotic phenotypes triggered by overexpression of ARHGAP19 depended upon the arginine 143 of the GAP domain suggested that effects of ARHGAP19 on cytokinesis occur through regulation of one or several GTPases. By performing a GAP assay *in vitro*, we found that WT ARHGAP19 was able to stimulate the GTP hydrolysis catalysed by RhoA, but not by Rac1 or CDC42 (Fig. 5A). Thus, ARHGAP19 can function as a GAP protein for RhoA. As expected, the R143A mutant of ARHGAP19 displayed no GAP activity.

We obtained additional evidence that ARHGAP19 can regulate RhoA *in vivo*. A cytoplasmic mutant of GFP-ARHGAP19, truncated of its C-terminal region [which contains two potential bi-partite nuclear localisation signal (NLS) sequences] (supplementary material Fig. S3), was expressed in HeLa cells, in which endogenous ARHGAP19 protein was hardly detectable (as assessed by RT-PCR analysis of mRNA expression or immunoprecipitation and western blot experiments performed in conditions similar to those used with lymphocytes in Fig. 3A). Expression of GFP-ARHGAP19-ΔCter decreased cellular levels of active RhoA (but not Rac1 or CDC42) assessed by pull-down experiments using unsynchronised cells (Fig. 5B), decreased stress fibres in interphasic cells (an event known to lie downstream of RhoA activity) (Fig. 5C), and impaired the RhoA-dependent cell rounding (Fig. 5D) that normally occurs at the beginning of mitosis of adherent cells (Maddox and Burridge, 2003). As expected, all these effects depended upon arginine 143 of the GAP domain of ARHGAP19.

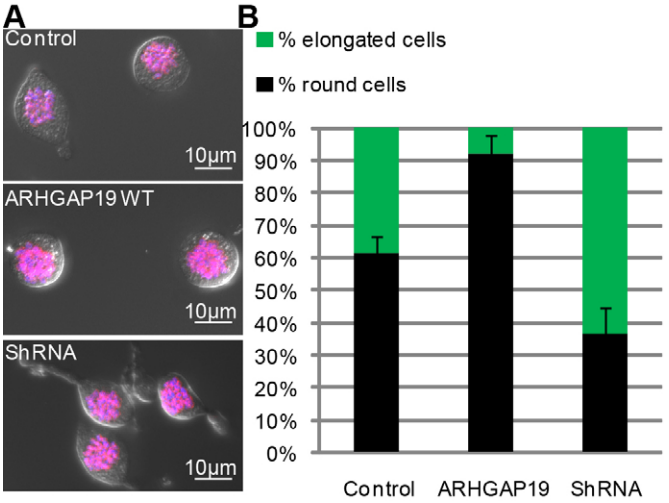

Fig. 4. Manipulation of ARHGAP19 levels impacts cell shape in cells blocked in prometaphase by treatment with nocodazole. Lymphocytes (control, ARHGAP19-overexpressing or ARHGAP19-depleted) were synchronised in G1 by IL-2 withdrawal for 2 days, after which cell cycling was resumed by addition of IL-2 for 24 hours. Cells about to enter mitosis were then treated with nocodazole for 5 hours. Cells were fixed using paraformaldehyde, and labelled for DNA (Hoechst, blue) and phospho-histone-H3 (red). (A) Representative fields for each population are shown. (B) For each population, more than 150 cells in random fields of three independent experiments were analysed. The histogram shows mean ± s.e.m. percentages of elongated or round cells.

Journal of Cell Science (2014) 127, 400–410 doi:10.1242/jcs.135079

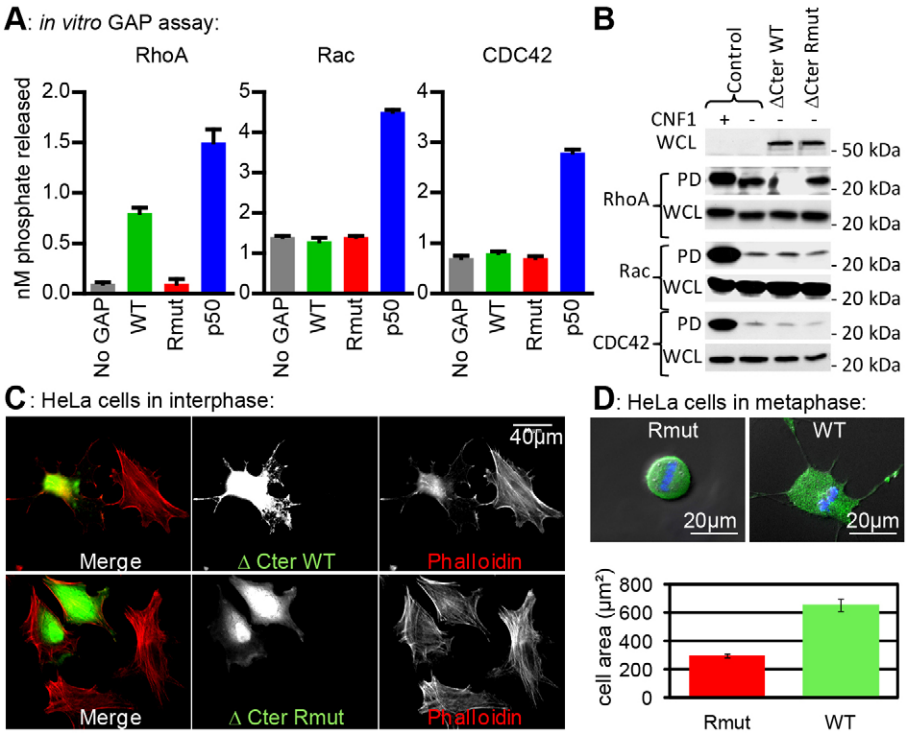

Fig. 5. ARHGAP19 displays GAP activity on RhoA, but not Rac1 or CDC42. (A) *In vitro* assay assessing the ability of ARHGAP19 to promote GTPase-mediated GTP hydrolysis. The histogram displays the amount of inorganic phosphate released by recombinant GTPases, in the absence or the presence of GFP-ARHGAP19 (WT or Rmut) purified by immunoprecipitation from mitotic Kit225 lymphocytes, or of recombinant p50RhoGAP used here as a positive control. (B–D) WT or Rmut forms of truncated GFP-ARHGAP19 (GFP-ARHGAP19-ΔCter) were expressed in HeLa cells. (B) Pull-down (PD) experiments using lysates of HeLa cells expressing the WT or Rmut forms of GFP-ARHGAP19-ΔCter. GST-Rho Binding Domain of Rhotekin (GST-RBD) or GST-CRIB of PAK (GST-CRIB) were used to pull-down active RhoA or active Rac1 and CDC42, respectively. Thus, western blots on the PD lanes reveal levels of active GTPases, whereas western blots on the whole cell lysate (WCL) lanes show total levels of the indicated GTPases. As a positive control, untransfected HeLa cells were treated for 30 minutes with CNF1, a bacterial toxin that induces deamination of the catalytic glutamine of the Rho GTPases and thus prevents them from hydrolysing GTP. (C,D) Transfected HeLa cells were seeded onto glass coverslips coated with laminin, and then fixed with paraformaldehyde. (C) DNA and polymerised actin-containing structures were stained with Hoechst (blue) and Phalloidin (red), respectively. Expression of the WT, but not the Rmut form, decreased occurrence of stress fibres, compared with adjacent, untransfected cells. (D) At the metaphase stage, untransfected HeLa cells (not shown) or cells expressing GFP-ARHGAP19-ΔCter Rmut (top panel) were round and displayed a loosened adherence to the extracellular matrix, whereas cells expressing GFP-ARHGAP19-ΔCter WT (bottom panel) remained fully adherent and flat. Histogram represents surface areas of these cells in metaphase (mean ± s.e.m.; $n=24$ for each population).

The level and activity of ARHGAP19 affect recruitment of RhoA, citron and myosin II at the cell equator, and regulate Rock2-mediated phosphorylation of vimentin in early mitosis

To investigate the molecular mechanisms through which ARHGAP19 controls lymphocyte division, we assessed effects of manipulation of ARHGAP19 levels or activity on the subcellular localisations of RhoA (the direct target of ARHGAP19), citron and Rock [known effector kinases of RhoA involved in cytokinesis (D'Avino et al., 2004; Gruneberg et al., 2006; Kosako et al., 2000; Madaule et al., 1998)], and myosin IIA [a protein involved in cytoskeleton contractility and whose membrane recruitment during cytokinesis is dependent on Rock- and/or citron-mediated phosphorylation of the myosin light chain subunit (Uehara et al., 2010)].

In control lymphocytes, RhoA, citron and myosin IIA were recruited to the equatorial membrane at anaphase onset and concentrated in the ingressing cleavage furrow afterwards (Fig. 6A–D), as reported in other cell types. Overexpression of WT ARHGAP19 drastically decreased membrane recruitment of RhoA, citron and myosin IIA (Fig. 6A–D). Conversely, silencing of *ARHGAP19*, or expression of its dominant-negative R143A mutant, clearly enhanced membrane recruitment of RhoA, citron and myosin IIA in about 50% of the cells at the prophase and metaphase stages (Fig. 6A–D). Such increases might also occur to some extent at later mitotic stages, although staining quantification did not reveal statistical differences.

Staining of lymphocytes with the anti-phospho-S1366 Rock2 antibody that recognises specifically the activated, autophosphorylated form of Rock2 (Chuang et al., 2012) revealed its striking localisation on a cage-like subcellular structure (Fig. 7A). This structure is reminiscent of that formed in lymphocytes by the vimentin intermediate filaments (Brown et al., 2001), which can be phosphorylated by Rock (Goto et al., 1998). We observed that active Rock2 (stained in green) and pS71-vimentin (stained in red) globally colocalised (Fig. 7A), although intensity variations of the two signals did not fully correlate (Fig. 7B), making it unlikely that the anti-active Rock2 antibody crossreacted with phosphorylated vimentin. In addition, reciprocal immunoprecipitation and western blot experiments (not shown) confirmed that these two antibodies did not crossreact. Global variations in levels of active Rock2 and pS71-vimentin correlated during mitosis progression (Fig. 7A). Indeed, in control lymphocytes, active Rock2 and pS71-vimentin were readily

Journal of Cell Science (2014) 127, 400–410 doi:10.1242/jcs.135079

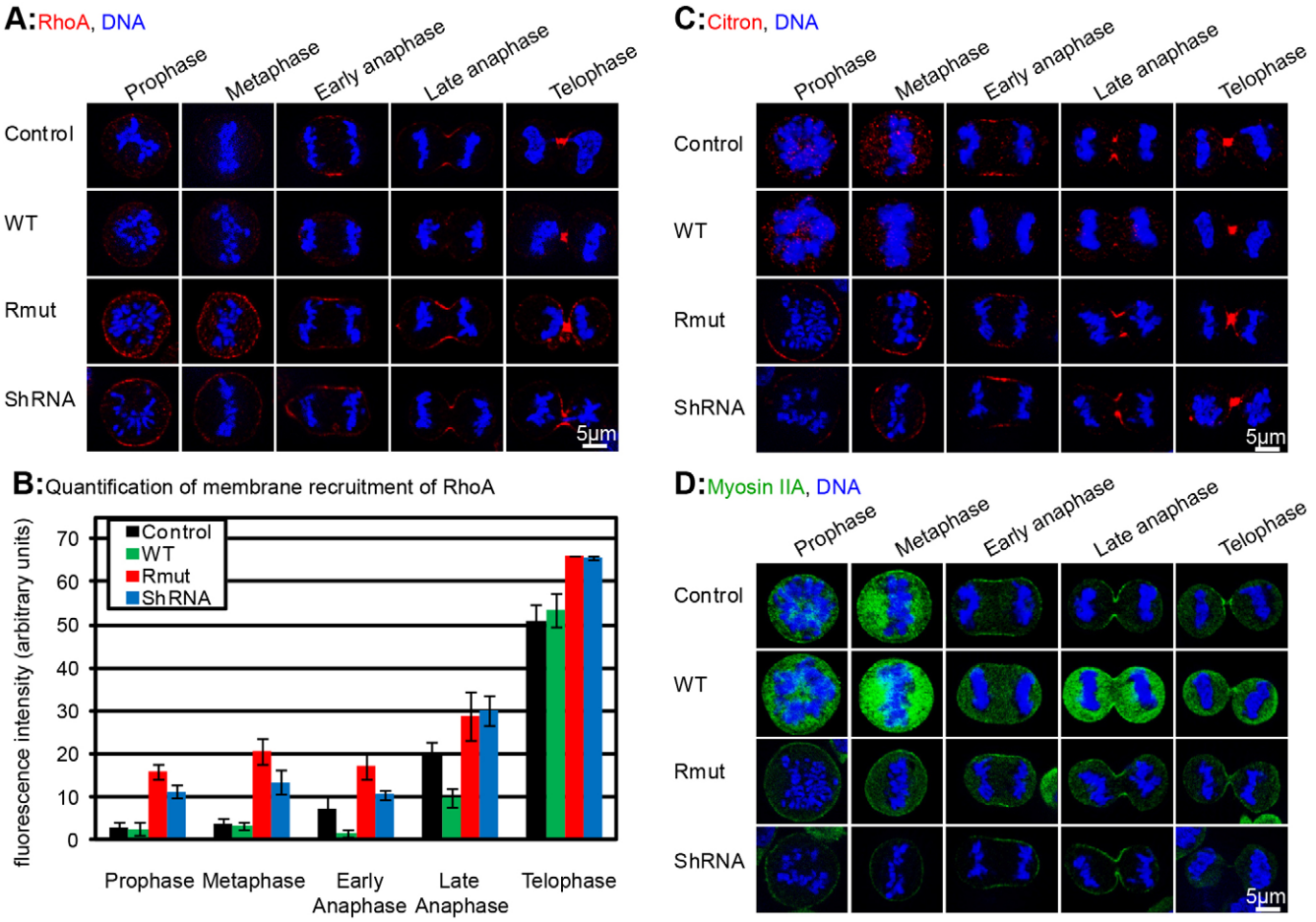

Fig. 6. Manipulation of the level and activity of ARHGAP19 affect the cell membrane recruitment of RhoA, citron and myosin II, especially during the first steps of mitosis (from prophase to early anaphase). (A,C,D) Kit225 lymphocytes (control, expressing the WT or Rmut forms of ARHGAP19, or depleted in ARHGAP19) were fixed using TCA. Cells were labelled for DNA (Hoechst, blue) and RhoA (red in A), citron (red in C) or myosin II (green in D). Each panel shows optical sections corresponding to the median plane of the mitotic cells. For the red and green channels, exposure times during picture acquisition (linear mode) were kept constant from one population to the other. Moreover, image post-treatments (e.g. contrast adjustments) were performed after combination of all the individual pictures into one. Thus, relative intensities reflect actual variations of staining according to the mitotic stage or the status of ARHGAP19 expression or activity. (B) Quantification of RhoA recruitment to the membrane of dividing lymphocytes. For mitotic stages from metaphase to telophase, fluorescence intensities were measured at the equatorial membranes. For cells in prophase, fluorescence intensities were measured at random membrane positions. Average fluorescence intensities in the cytoplasm were subtracted from membrane fluorescence intensities to obtain values representing RhoA enrichment to membranes. Data are expressed as mean ± s.e.m. $n>10$ for each mitotic stage of each cell population.

detectable on the cage at the prophase and metaphase stages, and in the intercellular bridges separating daughter cells in telophase. Overexpression of WT ARHGAP19 drastically decreased levels of active Rock2 and pS71-vimentin in prophase and metaphase. Conversely, levels of active Rock2 and pS71-vimentin were increased by silencing of *ARHGAP19* or expression of its dominant-negative R143A mutant at the prophase and metaphase stages, and were still readily detectable in anaphase. Thus, compared with control cells, ARHGAP19-deficient lymphocytes displayed increased, and possibly prolonged, levels of active Rock2 and pS71-vimentin. Phosphorylation of vimentin has been described to increase flexibility of the cage subtending the plasma membrane (Inagaki et al., 1987), which is required for major morphological changes to occur in lymphocytes (Paulin-Levasseur and Brown, 1987). Thus, the ability of ARHGAP19 to regulate the RhoA/Rock2-dependent phosphorylation of vimentin probably represents one of the mechanisms through which ARHGAP19 controls cell shape changes in early mitosis of lymphocytes.

DISCUSSION

We report here that ARHGAP19, a previously uncharacterised protein, has a crucial role in T lymphocyte division. The *ARHGAP19* gene is expressed predominantly in cells of hematopoietic origin, with the noticeable exception of germ cells. This might explain why it has escaped identification in the previous, large scale siRNA-based screens seeking for genes involved in division of epithelial cells or fibroblasts. We observed that ARHGAP19 controls two aspects of lymphocyte division: time of morphological changes in early mitosis, and chromosome segregation in anaphase.

Action of ARHGAP19 throughout cell division

The sole existing clues regarding the molecular actors controlling mitotic cell elongation in early mitosis come from studies using *Drosophila* S2 cells. In these cells, depletion of Rock or myosin II using siRNA impaired cell elongation in early anaphase, decreased mitotic cell blebbing and delayed formation of

Journal of Cell Science (2014) 127, 400–410 doi:10.1242/jcs.135079

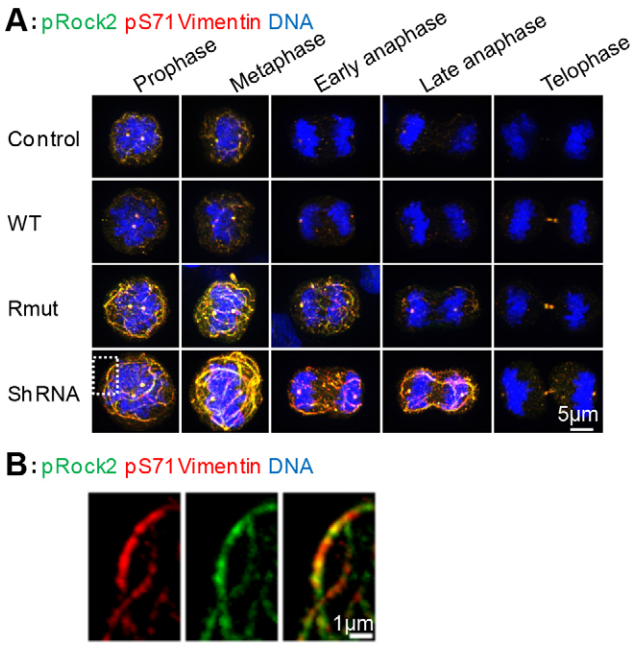

Fig. 7. Manipulation of the level or activity of ARHGAP19 affects Rock2 activity as well as the phosphorylation status of its vimentin substrate with which it colocalises. Kit225 lymphocytes (control, expressing the WT or Rmut forms of ARHGAP19, or depleted in ARHGAP19) were fixed using trichloroacetic acid. Cells were labelled for DNA (Hoechst, blue), phospho-Rock2 (green) and phospho-S71-vimentin (red). (A) Overlaid image showing colocalisation (yellow) of phospho-Rock2 and phospho-vimentin. For the red and green channels, exposure times during picture acquisitions (linear mode) were kept constant from one population to the other. *z*-stack projections across the entire cell thickness are shown. Imaging post treatment (e.g. contrast adjustments) was performed after combination of all the individual pictures into one. Thus, relative intensities reflect actual variations of staining according to the mitotic stage or the status of ARHGAP19 expression or activity. (B) Higher magnification image of the rectangle-delimited region of the ARHGAP19-depleted lymphocyte in prophase shown in A, which illustrates that intensity variations of the two signals do not always correlate (i.e. higher levels of red or green signals are detected depending on the portion of vimentin filament considered).

cleavage furrows (Hickson et al., 2006). The morphological phenotypes we observed in lymphocytes overexpressing WT ARHGAP19 are reminiscent of those described when the Rock–myosin-II pathway is altered in S2 cells. In addition, we found that ARHGAP19 acts as a GAP for RhoA in early mitosis, and controls the recruitment of citron and myosin II at the plasma membrane, which is crucial for cytoskeleton contractility. Furthermore, ARHGAP19 controls Rock2-mediated phosphorylation of vimentin, which is an essential determinant of the stiffness and shape of lymphocytes. This ARHGAP19-regulated RhoA–Rock-2–vimentin signalling pathway that occurs in early mitosis of lymphocytes has not been described in adherent cells, in which pS71-vimentin was found only during anaphase (in the ingressing furrow) or telophase (in the intercellular bridge) (Goto et al., 1998; Kosako et al., 1999; Yasui et al., 2001), and might be a characteristic of cells dividing in suspension.

In addition to cell elongation, cleavage furrow ingression also occurred earlier in ARHGAP19-deficient lymphocytes than in control cells. The excessively elongated shape in early mitosis could be sufficient to promote early furrow ingression by bringing the spindle and the cell cortex into close proximity (Rappaport and Rappaport, 1993; Shuster and Burgess, 1999; Shuster and Burgess, 2002). The increased recruitment of myosin II at the plasma membrane, which favours cytoskeleton contractility, is an alternative or complementary explanation for early cleavage furrow ingression. In adherent cells, RhoA activity is required for de-adhesion and rounding up at the onset of mitosis. The obvious inference of our results is that in lymphocytes where these steps are not needed, RhoA activity must be restrained to prevent precocious morphological changes. We propose that some of the ARHGAP19-regulated pathways serve to delay these changes in cell shape (including furrow ingression) until chromosomes segregate away from the cell mid-zone during anaphase.

In 43.6% of ARHGAP19-deficient lymphocytes, lagging DNA was observed during furrow ingression. Others have shown that the CDC42 member of the Rho GTPase family, but not RhoA, controls chromosome segregation in other cell types, by regulating maintenance of centromeres (Lagana et al., 2010), attachment of microtubules to kinetochores (Oceguera-Yanez et al., 2005; Yasuda et al., 2004) and spindle morphology (Ban et al., 2004). The p190B RhoGAP-dependent modulation of Rac activity has also been shown recently to regulate attachment of microtubules to kinetochores (Hwang et al., 2012). However, ARHGAP19 did not act on CDC42 or Rac (Fig. 5A,B). Moreover, analysis of the spindle structure in ARHGAP19-deficient lymphocytes did not reveal major defects (supplementary material Fig. S4). Finally, staining of ARHGAP19-deficient lymphocytes with anti-phospho-CENPA or anti-BuBR1 antibodies revealed that both proteins are present on kinetochores during prophase, and absent in cells in anaphase, even in those with massive chromatin bridges (not shown). Thus, depletion of ARHGAP19 does not seem to affect the activation of the spindle assembly checkpoint that normally occurs in early mitosis, nor does it allow mitotic slippage in the presence of an unsatisfied checkpoint (Brito and Rieder, 2006). Consistent with these notions, the lagging DNA events observed through videomicroscopy monitoring of ARHGAP19-depleted lymphocytes did not look like chromosomes ‘left behind’ as a result of defective attachment of microtubules to centromeres or their detachment during chromosome poleward segregation. Instead, 44% of the ARHGAP19-deficient lymphocytes showed chromosome bridges occurring from the beginning of anaphase onset (in mild scenarios), or an apparent enlargement of the metaphasic chromosome plate as if sister chromatids were subject to forces pulling them apart but were not able to separate (in cells with the most severe phenotypes). These observations look similar to those described in cells with impaired topoisomerase II activity (which results in inhibition of DNA decatenation and physically prevents sister chromatid separation) (Spence et al., 2007). How the RhoA hyperactivation that results from depletion of ARHGAP19 might affect chromatin organisation or chromosome separation remains to be elucidated.

Although the existence of variations in ARHGAP19 levels in leukaemic T cells, revealed through our transcriptome analysis, might be circumstantial, we do not exclude the notion that the genomic instability resulting from ARHGAP19 malfunction might participate in the leukaemic process. Further investigations will be required to characterise the mechanisms underlying the chromosome mis-segregation induced by the silencing of *ARHGAP19* in lymphocytes.

Spatiotemporal regulation of RhoA and ARHGAP19, and possible feedback

Plasma membrane recruitment of RhoA was different in dividing lymphocytes expressing the WT or Rmut forms of

Journal of Cell Science (2014) 127, 400–410 doi:10.1242/jcs.135079

GFP-ARHGAP19. This indicates that ARHGAP19 activity impacts localisation of RhoA. Because plasma membrane recruitment of RhoA is known to reflect its activation status (Nishimura and Yonemura, 2006; Piekny et al., 2005), and since ARHGAP19 displays a GAP activity on RhoA, this observation was not surprising. Less expected was the finding that spatiotemporal plasma membrane recruitment of ARHGAP19 itself was linked to its activity and/or to downstream events. ARHGAP19 (endogenous, or fused to GFP in its WT or Rmut forms) was nuclear before mitosis onset, scattered in the cytoplasm after nuclear envelope breakdown and at some point, relocalised to the plasma membrane (Fig. 2; Fig. 3C,E and supplementary material Movies 2 and 4). Strikingly, Rmut GFP-ARHGAP19 was recruited to the membrane earlier than WT GFP-ARHGAP19, and whereas the main areas of Rmut GFP-ARHGAP19 recruitment were the cell equator and then the ingressing furrow, the most remarkable relocalisation of WT GFP-ARHGAP19 was at the poles of the dividing lymphocytes.

During live observation of lymphocytes expressing Rmut GFP-ARHGAP19, plasma membrane recruitment of ARHGAP19 always occurred just before anaphase onset (in the cells dividing without major phenotypes) or precocious cell ingression. Analyses in fixed cells indicated that the zones of membrane recruitment of Rmut GFP-ARHGAP19 and RhoA globally coincided (supplementary material Fig. S5). Thus, the ability of active RhoA to interact with GAP proteins probably contributes to the recruitment of ARHGAP19 to the equatorial plasma membrane. Nevertheless, this model cannot account for the totality of our observations in dividing lymphocytes expressing WT GFP-ARHGAP19. The delay in membrane recruitment of WT GFP-ARHGAP19 could be explained by the decrease in RhoA activity. However, the relocalisation of WT GFP-ARHGAP19 to the poles of the dividing lymphocytes, which was repeatedly observed both in live and fixed cells, was never accompanied by enrichment of RhoA in these areas. Thus, although RhoA activation levels probably influence membrane recruitment of ARHGAP19, additional mechanisms must be at play. Many of the Rho pathway proteins involved in mitosis are regulated by phosphorylation (David et al., 2012), suggesting that the dynamic relocalisation of ARHGAP19 during the course of mitosis is under the control of one or several mitotic kinases. Regardless of the mechanisms responsible for sequestration of WT GFP-ARHGAP19 to the cell poles, this phenomenon might represent a regulatory feedback through which depletion of ARHGAP19 from the furrow area would alleviate the interference with cleavage furrow ingression resulting from excessive GAP activity. Consistent with this hypothesis, relocalisation of WT GFP-ARHGAP19 to the cell poles always preceded and was immediately followed by cleavage furrow ingression (Fig. 3C and supplementary material Movie 2). Restricted localisation of endogenous ARHGAP19 to the poles was not observed in control cells (Fig. 2), possibly because such localisation is transient in cells performing cytokinesis without phenotypic delays in morphological changes. Delineation of the mechanisms responsible for interaction of ARHGAP19 with the membrane and those that restrict ARHGAP19 to specific membrane areas will be required to determine whether recruitment of ARHGAP19 to the cell poles occurs only in cells with excessive GAP activity, or also participates in focusing the zone of active RhoA in control cells (which is important for efficient furrowing).

MATERIALS AND METHODS

Transcriptome analysis

The collection of 100 samples of human T-cell acute lymphoblastic leukaemia and the microarray experiments were described previously (Soulier et al., 2005). We established a list of Affymetrix probes corresponding to 300 genes of the Rho GTPase pathways. Probes for which signals below background had been obtained in all the leukaemia samples, as well as those that showed no significant variations across samples were deleted from the list. Unsupervised, hierarchical 2D clustering was then performed with this shortened list of probes.

Cell culture

Human Kit225 lymphocytes (Hori et al., 1987) were cultured as previously described (Seguin et al., 2009). Transfected cells were selected in 1–2 µg/ml puromycin. GFP-ARHGAP19 expression was induced by overnight treatment with 2 µg/ml doxycyclin. To block their cycle in the G1 phase, lymphocytes were cultured in the absence of IL-2 for 36–48 hours. Cell cycle progression was then resumed by addition of IL-2. To enrich the population in prometaphase-blocked cells, 40 ng/ml nocodazole (Sigma-Aldrich, St Louis, MO) was added for 16 hours (starting 24 hours after addition of IL-2). Cells were then washed thoroughly and placed in culture medium containing IL-2 to allow progression through mitosis.

Human leukaemia Jurkat T cells (ACC 282) were obtained from DSMZ (Braunschweig, Germany) and cultured in Glutamax-containing RPMI 1640 medium supplemented with 10% fetal calf serum and 1 mM sodium pyruvate. In experiments involving stable transfection, Jurkat cells were selected and maintained in 1 µg/ml puromycin.

HeLa cells were obtained from ATCC and cultured in Glutamax-containing DMEM medium supplemented with 10% fetal calf serum and 1 mM sodium pyruvate. HeLa cells were transiently transfected using JetPEI transfection reagent (PolyPlus Transfection, Illkirch, France).

Plasmids

cDNA encoding human ARHGAP19 was generated by RT-PCR, using specific primers (5′-tcgaAGATCTATGGCGACTGAGGCACAGAG-3′ and 5′-accgGAATTCTGCATGGACCATAGGAGACA-3′) and RNA from Kit225 lymphocytes as a template, and cloned into the pEGFP-C1 (Clontech, Mountain View, CA) or pGEX4T2 (Pharmacia Biotech, Uppsala, Sweden) vectors between the *Bgl*II and *Eco*RI sites. Sequence analysis confirmed that the cloned ORF encodes the reference ARHGAP19 protein (SwissProt Q14CB8).

Where indicated, the R143 amino acid of ARHGAP19 was mutated using the QuikChange II XL Kit from Stratagene (La Jolla, CA), the forward primer CAAAAACTTGCGAGTAGAGGGTTTGTTTgcAGTA-CCGGGTAATAG and its reverse complement.

The pEGFP-ARHGAP19ΔCter construct encoding the truncated form of ARHGAP19, in which the last 169 amino acids are missing, was generated by digesting the pEGFP-ARHGAP19 plasmid with *Bam*HI and re-ligating it on itself.

In the pEGFP-Cter construct, the region encoding the C-terminal 169 amino acids of the canonical ARHGAP19 was placed in-frame with the EGFP coding region of the pEGFP-C1 vector. For this purpose, the pEGFP-C1 vector was digested with *Bgl*II and *Bam*HI, dephosphorylated using calf intestinal alkaline phosphatase (CIAP) and gel-purified. In parallel, the pEGFP-ARHGAP19 construct was digested with *Bam*HI and the resulting 522-nucleotide insert was gel-purified. Following ligation and plasmid amplification and purification, sequence analysis was performed to identify plasmids in which the 522-nucleotide insert was in the correct orientation.

To generate the plasmid allowing inducible expression of GFP-ARHGAP19, we digested the pEGFP-ARHGAP19 plasmid using *Age*I and *Eco*RI restriction enzymes and subcloned this insert into the pTRIPZ vector (OpenBiosystems, Thermo Fisher Scientific, Huntsville, AL).

Silencing of *ARHGAP19* expression was performed by transfection of pGIPZ plasmids from OpenBioSystems: the targeting sequences of the ‘Sh113’ and ‘Sh117’ short hairpins (mature antisenses) were TTAACTTTGTGATATTCTC and TAGGTATTGAGGAATACAG, respectively.

Purification of GST-ARHGAP19 protein and generation of anti-ARHGAP19 rabbit antibodies

KRX bacteria (Promega, Madison, WI) were transformed with the pGEX-ARHGAP19 plasmid. Expression of GST-ARHGAP19 was induced by IPTG for 4 hours at 37℃. Bacteria were lysed in a buffer containing 50 mM Tris-HCl, pH 7.5, 50 mM NaCl, 2 mM $MgCl_2$, 0.5% Triton X-100, 1 mM DTT, 2 mg/ml lysozyme and protease inhibitors, and sonicated. GST-ARHGAP19 fusion proteins were purified with glutathione-Sepharose beads (GE Healthcare, Uppsala, Sweden) and then eluted in the presence of 25 mM reduced glutathione, 100 mM Tris-HCl, pH 8, 150 mM NaCl, 1 mM DTT and 0.5% Triton X-100. Dialysis of eluted proteins was performed in a buffer containing 100 mM sodium bicarbonate, pH 8.4, 500 mM NaCl, 1 mM DTT and 0.5% Triton X-100.

GST-ARHGAP19 proteins were used as immunogen for Eurogentec (Angers, France) to produce rabbit antisera. Antibodies were purified by incubating whole serum with GST-ARHGAP19 proteins covalently coupled to CNBR beads (GE Healthcare). After extensive washing of the beads with two buffers (Buffer 1: 0.1 M sodium acetate, pH 4, 0.5 M NaCl, 0.5% Triton X-100; Buffer 2: 100 mM sodium bicarbonate, pH 8.4, 500 mM NaCl, 1 mM DTT and 0.5% Triton X-100), antibodies were eluted with 20 mM glycine, pH 2.5, and immediately supplemented with 0.1 volumes of 1 M Tris-HCl, pH 8.5. Antibodies were then dialysed in PBS overnight.

In vitro GAP assay

GFP-ARHGAP19 (WT or Rmut) was immunoprecipitated using GFP-Trap beads (Chromotek GMBH, Planegg-Martinsried, Germany) from doxycyclin-treated GFP-ARHGAP19-expressing Kit225 cells synchronised in prometaphase. Assay was performed using a kit from Cytoskeleton. (Denver, CO), according to the manufacturer's protocol.

RT-PCR

Total RNA from Kit225 lymphocytes were purified and subjected to RT-PCR using primers specific for ARHGAP19, RacGAP1, ECT2, NET1, CCNA2 or GAPDH. Primer sequences were: GGCCATTGGTGAA-TTGAAGG and TGCATGGACCATAGGAGACA for *ARHGAP19*; CA-GATAAGGGTCAATACGAAGTC and TCCCAACTAACAATAAAG-AGTAGGC for *RACGAP1*; CATTTGCTGTTTCAAAGTGTGA and GACAAACATTTGTAGCACTCCC for *ECT2*; TAGTCATAAGATG-GAAAAAG and GATCTATTTACAGTCTTTTC for *NET1*; AAATC-TGTAACAATGAAAGACTGCC and GATACCATAATTTGTACTTG-GCCT for *CCNA2*; ACCACAGTCCATGCCATCAC and TCCACCAC-CCTGTTGCTGTA for *GAPDH*. PCR products were run on agarose gels containing ethidium bromide and analysed under UV using a GelDoc system (BioRad, Hercules, CA).

Antibodies

Rabbit SY1985 anti-ARHGAP19 antibody was home made. Goat anti-RACGAP1 (ab2270), rat anti-phospho-S71 vimentin (TM71) and rabbit anti-phospho-Ser28 Histone H3 (ab32388) were from Abcam (Cambridge, UK). Rabbit anti-NET1 (ab2), rabbit anti-non-muscle myosin IIA and mouse anti-alpha-tubulin (DM1A) were from Sigma-Aldrich. Rabbit anti-ECT2 (sc-1005), mouse anti-Hsc70 (sc-7298), goat anti-citron (sc-1848), goat anti-ARHGAP19 (sc-104815) and mouse anti-RhoA (26C4) were from Santa Cruz Biotechnology (Santa Cruz, CA). Mouse anti-CDC42 (ACD03) was from Cytoskeleton Inc. (Denver, CO). Mouse anti-p190B RhoGAP (clone 54) and mouse anti-Rac1 (clone 102) were from BD Biosciences (Franklin Lakes, NJ). Rabbit anti-phospho-Ser1366 ROCK2 antibody (GTX122651) was from GeneTex (Irvine, CA). HRP-conjugated anti-mouse and anti-rabbit secondary antibodies were purchased from GE Healthcare (Uppsala, Sweden) and Cell Signaling Technology (Ipswich, MA), respectively. The secondary antibodies used for microscopy, conjugated to Alexa Fluor 488, Alexa Fluor 594 or Rhodamine Red, were from Molecular Probes (Eugene, OR).

Immunoprecipitation and western blotting

Lymphocytes were lysed in 50 mM Tris-HCl, pH 7.5, 0.5% NP40, 50 mM NaCl, 5 mM $MgCl_2$, 10 mM NaF, 2 mM NaPP, 1 mM NaV, 1 mM DTT, 25 nM Calyculin A (#208851, Calbiochem, La Jolla, CA), 25 nM okadaic acid (#459618, Calbiochem), 10 µM Mg132 (#474790, Calbiochem), 1 mM PMSF and protease inhibitors (#P8240, Sigma-Aldrich). For analysis of whole cell lysates, 50 µg of proteins were used. Immunoprecipitation of endogenous ARHGAP19 [using 1 µg of purified SY1985 antibody, 1 mg of whole cell lysates and Protein-G Sepharose beads (GE Healthcare)], polyacrylamide gel electrophoresis, wet transfer onto PVDF membranes (GE Healthcare) and western blotting were performed according to standard procedures.

Videomicroscopy

Unsynchronised lymphocytes were treated with the cell-permeable DNA stain Syto59 (3.75 nM; Molecular Probes) and settled on a coverslip-like surface (Ibidi 60 µ-Dishes 35 mm, high; Ibidi, Martinsried, Germany) coated with a suboptimal dose of poly-L-lysine (0.002% in PBS; Sigma-Aldrich) in order to limit their displacement during the time course of the experiment. Importantly, cells did not adopt an adherent morphology when using these settings. Cells were photographed every minute using the Fluoview FV10i-W confocal laser-scanning microscope (objective 60× NA 1.2), equipped with a built-in incubator. The environment in the culture chamber was maintained at 37℃, 90% humidity and 5% CO_2. Laser power was kept as low as possible (usually below 5%) to avoid potential detrimental effects on the cells. Acquired images were processed using ImageJ software (NIH).

Microscopy on fixed cells

Lymphocytes were fixed (in suspension) for 15 minutes using a solution of 4% paraformaldehyde in PBS at 37℃, or for 10 minutes using a solution of 10% trichloroacetic acid in water at 4℃. Cells were washed in PBS, incubated in a solution of 0.05 M NH_4Cl in PBS for 15 minutes and permeabilised with washing buffer (0.1% Triton X-100, 3% BSA, in PBS) for 10 minutes. Staining was achieved by two consecutive, 1 hour incubations in solutions containing the primary and secondary antibodies diluted in washing buffer. Cells were resuspended in 10 µl fluorescence-preserving mounting medium (Dako North America, Inc., Carpinteria, CA) containing 2.5 µg/ml Hoechst 33342 (Molecular Probes) and placed between glass slides and 24×24 mm coverslips. Cells were examined under a Zeiss AxioImager Z1 fluorescence upright microscope (Zeiss, Jena, Germany) equipped with motorised Z drive, apotome and 63× 1.40 oil M27 objective. Images were processed using ImageJ software. For experiments involving HeLa cells, the same protocol was followed, except that cells were first seeded onto glass coverslips coated with fibronectin, before fixation. Where indicated, 3.3 nM Alexa Fluor-594-conjugated Phalloidin (Molecular Probes) was applied to the fixed cells for 1 hour, to stain polymerised actin-containing structures.

Statistical analyses

Data were processed using GraphPad software to calculate means ± s.e.m. Unpaired, two-tailed Student's *t*-tests were performed to determine whether means were significantly different.

Acknowledgements

We thank Prof. F. Sigaux and Ligue Nationale Contre le Cancer (CIT® program) for providing access to the transcriptome data, Dr Aurélien de Reynies for performing the 2D clustering, Sophie Desnoulez from the Imagery Facility at IGR (PFIC) for her help with time-lapse microscopy, Khadie Kouyate and Pierre-Yves Desplanques for technical help, and Dr William Vainchenker for critical reading of the manuscript.

Competing interests

The authors declare no competing interests.

Author contributions

M.D.D. and J.B. designed the study, analysed the data and wrote the manuscript. M.D.D. carried out project planning and, together with D.P., performed the experiments.

Funding

This work was funded in part by INSERM; Ligue Nationale Contre le Cancer (Equipe labellisée); and Agence Nationale de la Recherche [grant number

BLAN06 2_135169]. D.P. has a PhD fellowship from Ligue Nationale Contre le Cancer.

Supplementary material

Supplementary material available online at
http://jcs.biologists.org/lookup/suppl/doi:10.1242/jcs.135079/-/DC1

References

Ban, R., Irino, Y., Fukami, K. and Tanaka, H. (2004). Human mitotic spindle-associated protein PRC1 inhibits MgcRacGAP activity toward Cdc42 during the metaphase. *J. Biol. Chem.* **279**, 16394-16402.

Bastos, R. N., Penate, X., Bates, M., Hammond, D. and Barr, F. A. (2012). CYK4 inhibits Rac1-dependent PAK1 and ARHGEF7 effector pathways during cytokinesis. *J. Cell Biol.* **198**, 865-880.

Birkenfeld, J., Nalbant, P., Bohl, B. P., Pertz, O., Hahn, K. M. and Bokoch, G. M. (2007). GEF-H1 modulates localized RhoA activation during cytokinesis under the control of mitotic kinases. *Dev. Cell* **12**, 699-712.

Brito, D. A. and Rieder, C. L. (2006). Mitotic checkpoint slippage in humans occurs via cyclin B destruction in the presence of an active checkpoint. *Curr. Biol.* **16**, 1194-1200.

Brown, M. J., Hallam, J. A., Colucci-Guyon, E. and Shaw, S. (2001). Rigidity of circulating lymphocytes is primarily conferred by vimentin intermediate filaments. *J. Immunol.* **166**, 6640-6646.

Chalamalasetty, R. B., Hümmer, S., Nigg, E. A. and Silljé, H. H. (2006). Influence of human Ect2 depletion and overexpression on cleavage furrow formation and abscission. *J. Cell Sci.* **119**, 3008-3019.

Chan, A. M., Takai, S., Yamada, K. and Miki, T. (1996). Isolation of a novel oncogene, NET1, from neuroepithelioma cells by expression cDNA cloning. *Oncogene* **12**, 1259-1266.

Chuang, H. H., Yang, C. H., Tsay, Y. G., Hsu, C. Y., Tseng, L. M., Chang, Z. F. and Lee, H. H. (2012). ROCKII Ser1366 phosphorylation reflects the activation status. *Biochem. J.* **443**, 145-151.

D'Avino, P. P., Savoian, M. S. and Glover, D. M. (2004). Mutations in sticky lead to defective organization of the contractile ring during cytokinesis and are enhanced by Rho and suppressed by Rac. *J. Cell Biol.* **166**, 61-71.

David, M., Petit, D. and Bertoglio, J. (2012). Cell cycle regulation of Rho signaling pathways. *Cell Cycle* **11**, 3003-3010.

Goto, H., Kosako, H., Tanabe, K., Yanagida, M., Sakurai, M., Amano, M., Kaibuchi, K. and Inagaki, M. (1998). Phosphorylation of vimentin by Rho-associated kinase at a unique amino-terminal site that is specifically phosphorylated during cytokinesis. *J. Biol. Chem.* **273**, 11728-11736.

Green, R. A., Paluch, E. and Oegema, K. (2012). Cytokinesis in animal cells. *Annu. Rev. Cell Dev. Biol.* **28**, 29-58.

Gruneberg, U., Neef, R., Li, X., Chan, E. H., Chalamalasetty, R. B., Nigg, E. A. and Barr, F. A. (2006). KIF14 and citron kinase act together to promote efficient cytokinesis. *J. Cell Biol.* **172**, 363-372.

Hickson, G. R., Echard, A. and O'Farrell, P. H. (2006). Rho-kinase controls cell shape changes during cytokinesis. *Curr. Biol.* **16**, 359-370.

Hori, T., Uchiyama, T., Tsudo, M., Umadome, H., Ohno, H., Fukuhara, S., Kita, K. and Uchino, H. (1987). Establishment of an interleukin 2-dependent human T cell line from a patient with T cell chronic lymphocytic leukemia who is not infected with human T cell leukemia/lymphoma virus. *Blood* **70**, 1069-1072.

Hwang, M., Peddibhotla, S., McHenry, P., Chang, P., Yochum, Z., Park, K. U., Sears, J. C. and Vargo-Gogola, T. (2012). P190B RhoGAP Regulates Chromosome Segregation in Cancer Cells. *Cancers (Basel)* **4**, 475-489.

Inagaki, M., Nishi, Y., Nishizawa, K., Matsuyama, M. and Sato, C. (1987). Site-specific phosphorylation induces disassembly of vimentin filaments in vitro. *Nature* **328**, 649-652.

Jaffe, A. B. and Hall, A. (2005). Rho GTPases: biochemistry and biology. *Annu. Rev. Cell Dev. Biol.* **21**, 247-269.

Kamijo, K., Ohara, N., Abe, M., Uchimura, T., Hosoya, H., Lee, J. S. and Miki, T. (2006). Dissecting the role of Rho-mediated signaling in contractile ring formation. *Mol. Biol. Cell* **17**, 43-55.

Kittler, R., Pelletier, L., Heninger, A. K., Slabicki, M., Theis, M., Miroslaw, L., Poser, I., Lawo, S., Grabner, H., Kozak, K. et al. (2007). Genome-scale RNAi profiling of cell division in human tissue culture cells. *Nat. Cell Biol.* **9**, 1401-1412.

Kosako, H., Goto, H., Yanagida, M., Matsuzawa, K., Fujita, M., Tomono, Y., Okigaki, T., Odai, H., Kaibuchi, K. and Inagaki, M. (1999). Specific accumulation of Rho-associated kinase at the cleavage furrow during cytokinesis: cleavage furrow-specific phosphorylation of intermediate filaments. *Oncogene* **18**, 2783-2788.

Kosako, H., Yoshida, T., Matsumura, F., Ishizaki, T., Narumiya, S. and Inagaki, M. (2000). Rho-kinase/ROCK is involved in cytokinesis through the phosphorylation of myosin light chain and not ezrin/radixin/moesin proteins at the cleavage furrow. *Oncogene* **19**, 6059-6064.

Lagana, A., Dorn, J. F., De Rop, V., Ladouceur, A. M., Maddox, A. S. and Maddox, P. S. (2010). A small GTPase molecular switch regulates epigenetic centromere maintenance by stabilizing newly incorporated CENP-A. *Nat. Cell Biol.* **12**, 1186-1193.

Loria, A., Longhini, K. M. and Glotzer, M. (2012). The RhoGAP domain of CYK-4 has an essential role in RhoA activation. *Curr. Biol.* **22**, 213-219.

Madaule, P., Eda, M., Watanabe, N., Fujisawa, K., Matsuoka, T., Bito, H., Ishizaki, T. and Narumiya, S. (1998). Role of citron kinase as a target of the small GTPase Rho in cytokinesis. *Nature* **394**, 491-494.

Maddox, A. S. and Burridge, K. (2003). RhoA is required for cortical retraction and rigidity during mitotic cell rounding. *J. Cell Biol.* **160**, 255-265.

Mendoza, M., Norden, C., Durrer, K., Rauter, H., Uhlmann, F. and Barral, Y. (2009). A mechanism for chromosome segregation sensing by the NoCut checkpoint. *Nat. Cell Biol.* **11**, 477-483.

Miller, A. L., von Dassow, G. and Bement, W. M. (2008). Control of the cytokinetic apparatus by flux of the Rho GTPases. *Biochem. Soc. Trans.* **36**, 378-380.

Moffat, J., Grueneberg, D. A., Yang, X., Kim, S. Y., Kloepfer, A. M., Hinkle, G., Piqani, B., Eisenhaure, T. M., Luo, B., Grenier, J. K. et al. (2006). A lentiviral RNAi library for human and mouse genes applied to an arrayed viral high-content screen. *Cell* **124**, 1283-1298.

Neumann, B., Held, M., Liebel, U., Erfle, H., Rogers, P., Pepperkok, R. and Ellenberg, J. (2006). High-throughput RNAi screening by time-lapse imaging of live human cells. *Nat. Methods* **3**, 385-390.

Neumann, B., Walter, T., Hériché, J. K., Bulkescher, J., Erfle, H., Conrad, C., Rogers, P., Poser, I., Held, M., Liebel, U. et al. (2010). Phenotypic profiling of the human genome by time-lapse microscopy reveals cell division genes. *Nature* **464**, 721-727.

Nishimura, Y. and Yonemura, S. (2006). Centralspindlin regulates ECT2 and RhoA accumulation at the equatorial cortex during cytokinesis. *J. Cell Sci.* **119**, 104-114.

Norden, C., Mendoza, M., Dobbelaere, J., Kotwaliwale, C. V., Biggins, S. and Barral, Y. (2006). The NoCut pathway links completion of cytokinesis to spindle midzone function to prevent chromosome breakage. *Cell* **125**, 85-98.

Oceguera-Yanez, F., Kimura, K., Yasuda, S., Higashida, C., Kitamura, T., Hiraoka, Y., Haraguchi, T. and Narumiya, S. (2005). Ect2 and MgcRacGAP regulate the activation and function of Cdc42 in mitosis. *J. Cell Biol.* **168**, 221-232.

Paulin-Levasseur, M. and Brown, D. L. (1987). Vimentin dynamics during the mitogenic stimulation of mouse splenic lymphocytes. *Cell Motil. Cytoskeleton* **8**, 227-237.

Piekny, A., Werner, M. and Glotzer, M. (2005). Cytokinesis: welcome to the Rho zone. *Trends Cell Biol.* **15**, 651-658.

Rappaport, R. and Rappaport, B. N. (1993). Duration of division-related events in cleaving sand dollar eggs. *Dev. Biol.* **158**, 265-273.

Seguin, L., Liot, C., Mzali, R., Harada, R., Siret, A., Nepveu, A. and Bertoglio, J. (2009). CUX1 and E2F1 regulate coordinated expression of the mitotic complex genes Ect2, MgcRacGAP, and MKLP1 in S phase. *Mol. Cell. Biol.* **29**, 570-581.

Shuster, C. B. and Burgess, D. R. (1999). Parameters that specify the timing of cytokinesis. *J. Cell Biol.* **146**, 981-992.

Shuster, C. B. and Burgess, D. R. (2002). Transitions regulating the timing of cytokinesis in embryonic cells. *Curr. Biol.* **12**, 854-858.

Soulier, J., Clappier, E., Cayuela, J. M., Regnault, A., García-Peydró, M., Dombret, H., Baruchel, A., Toribio, M. L. and Sigaux, F. (2005). HOXA genes are included in genetic and biologic networks defining human acute T-cell leukemia (T-ALL). *Blood* **106**, 274-286.

Spence, J. M., Phua, H. H., Mills, W., Carpenter, A. J., Porter, A. C. and Farr, C. J. (2007). Depletion of topoisomerase IIalpha leads to shortening of the metaphase interkinetochore distance and abnormal persistence of PICH-coated anaphase threads. *J. Cell Sci.* **120**, 3952-3964.

Steigemann, P., Wurzenberger, C., Schmitz, M. H., Held, M., Guizetti, J., Maar, S. and Gerlich, D. W. (2009). Aurora B-mediated abscission checkpoint protects against tetraploidization. *Cell* **136**, 473-484.

Su, L., Pertz, O., Mikawa, M., Hahn, K. and Parsons, S. J. (2009). p190RhoGAP negatively regulates Rho activity at the cleavage furrow of mitotic cells. *Exp. Cell Res.* **315**, 1347-1359.

Tatsumoto, T., Xie, X., Blumenthal, R., Okamoto, I. and Miki, T. (1999). Human ECT2 is an exchange factor for Rho GTPases, phosphorylated in G2/M phases, and involved in cytokinesis. *J. Cell Biol.* **147**, 921-928.

Uehara, R., Goshima, G., Mabuchi, I., Vale, R. D., Spudich, J. A. and Griffis, E. R. (2010). Determinants of myosin II cortical localization during cytokinesis. *Curr. Biol.* **20**, 1080-1085.

Wu, D., Asiedu, M., Adelstein, R. S. and Wei, Q. (2006). A novel guanine nucleotide exchange factor MyoGEF is required for cytokinesis. *Cell Cycle* **5**, 1234-1239.

Yamada, T., Hikida, M. and Kurosaki, T. (2006). Regulation of cytokinesis by mgcRacGAP in B lymphocytes is independent of GAP activity. *Exp. Cell Res.* **312**, 3517-3525.

Yasuda, S., Oceguera-Yanez, F., Kato, T., Okamoto, M., Yonemura, S., Terada, Y., Ishizaki, T. and Narumiya, S. (2004). Cdc42 and mDia3 regulate microtubule attachment to kinetochores. *Nature* **428**, 767-771.

Yasui, Y., Goto, H., Matsui, S., Manser, E., Lim, L., Nagata Ki, and Inagaki, M. (2001). Protein kinases required for segregation of vimentin filaments in mitotic process. *Oncogene* **20**, 2868-2876.

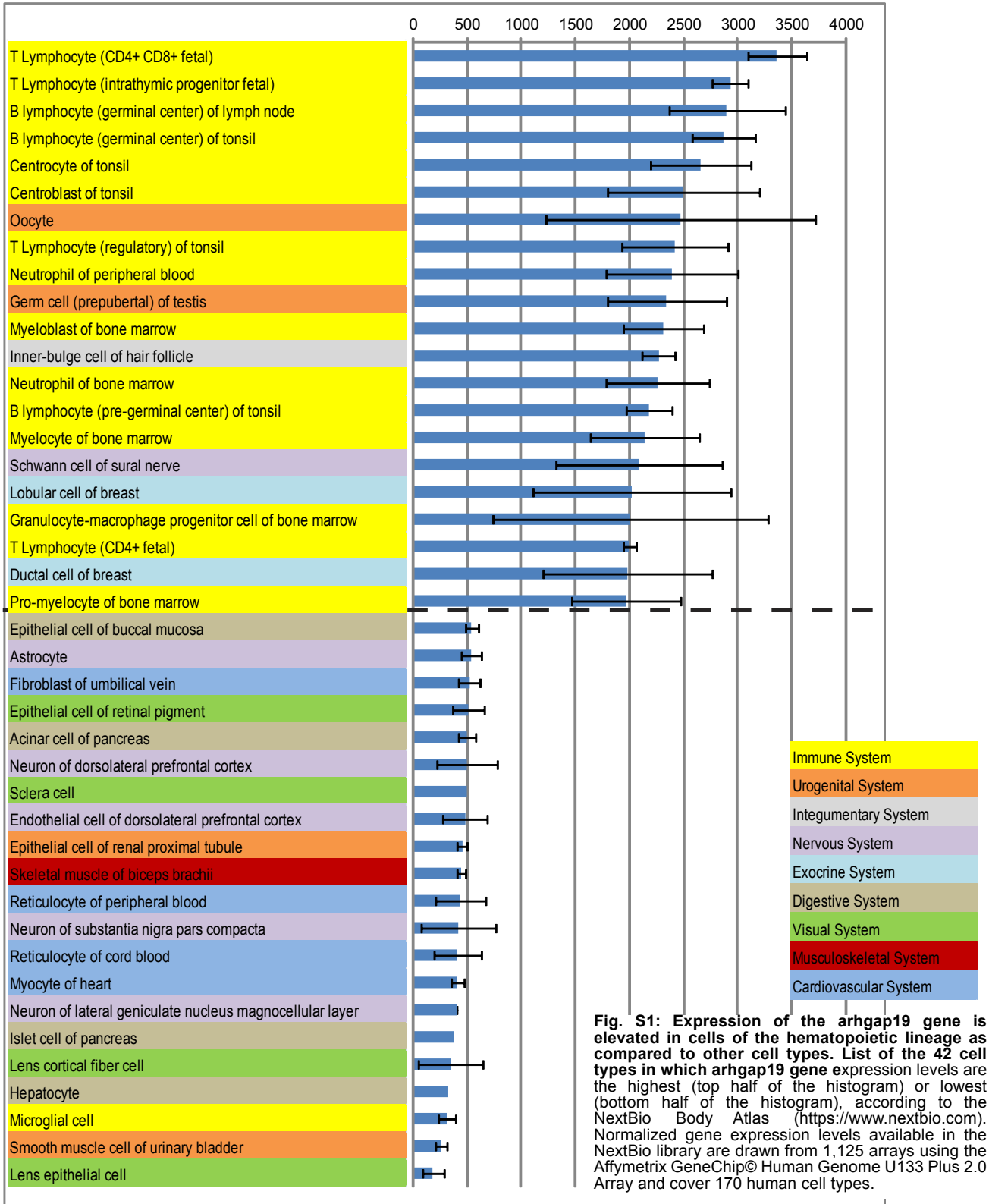

Fig. S1: Expression of the arhgap19 gene is elevated in cells of the hematopoietic lineage as compared to other cell types. List of the 42 cell types in which arhgap19 gene expression levels are the highest (top half of the histogram) or lowest (bottom half of the histogram), according to the NextBio Body Atlas (https://www.nextbio.com). Normalized gene expression levels available in the NextBio library are drawn from 1,125 arrays using the Affymetrix GeneChip© Human Genome U133 Plus 2.0 Array and cover 170 human cell types.

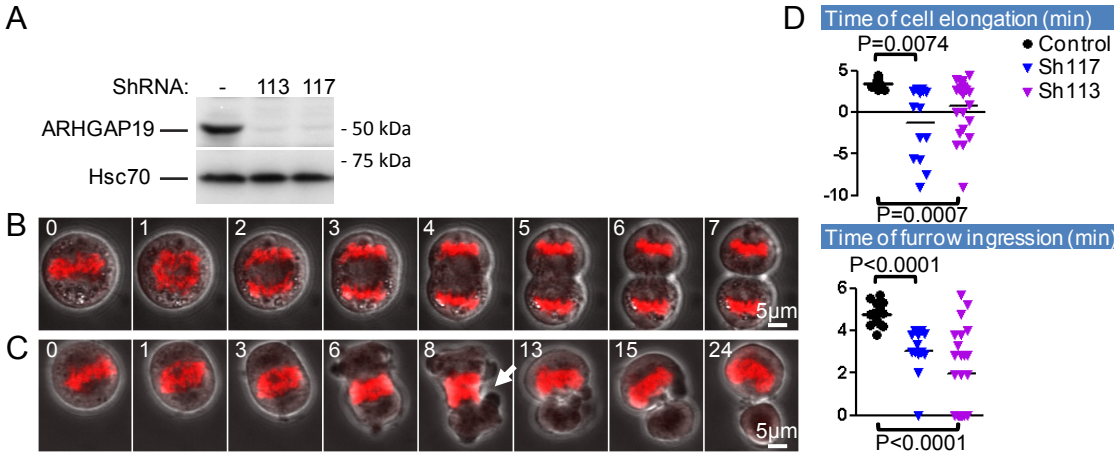

Fig. S2: Downregulation of ARHGAP19 levels in Jurkat lymphocytes through ShRNA induces excessive cell shape changes in early mitosis as well as chromosome segregation defects in anaphase. Jurkat T cells were stably transfected with plasmids bearing ShRNA against ARHGAP19 (Sh113 or Sh117). (**A**) Western blot analysis on the cell lysates was performed with our anti-ARHGAP19 antibody. Equal loading was confirmed by reprobing the blot with an anti-Hsc70 antibody. (**B, C**) Mitosis of a control Jurkat T cell (**B**) and of an ARHGAP-19-depleted Jurkat T cell (**C**), monitored by time-lapse microscopy. The red color corresponds to the fluorescence emitted by the DNA labeling, Syto 59 dye. Time "0 min" was set on the last frame displaying the cell in the metaphase stage. White arrow points out lagging DNA.(**D**) ARHGAP19 silencing induces precocious cell elongation and cleavage furrow ingression in Jurkat cells.

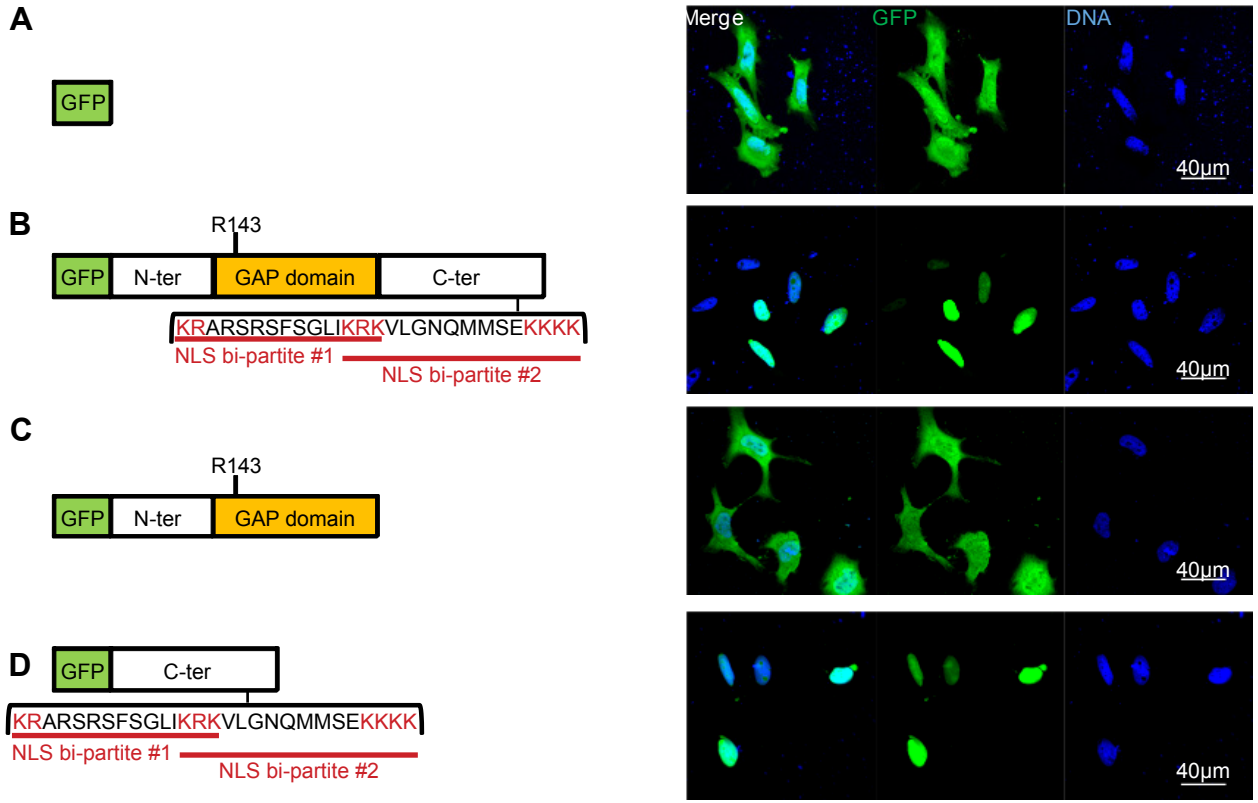

Fig. S3: Nuclear localization of ARHGAP19 depends on its C-terminal region. HeLa cells were transiently transfected with plasmids coding for GFP (**A**), GFP-ARHGAP19 full length (**B**), a truncated form of ARHGAP19 devoid of its C-terminal region (GFP-ARHGAP19- Cter) (**C**), or GFP fused to the C-terminal region of ARHGAP19 (GFP+Cter) (**D**). Schemes on the left part of the figure illustrate the primary structure of these proteins and the respective localizations of the GAP domain and of the two potential overlapping bi-partite nuclear localization signals (NLS). ARHGAP19 truncated of its C-terminal region is no longer enriched in the cell nucleus (**C**). Reciprocally, fusion with the C-terminal region of ARHGAP19 is sufficient to target GFP to the cell nucleus (**D**).

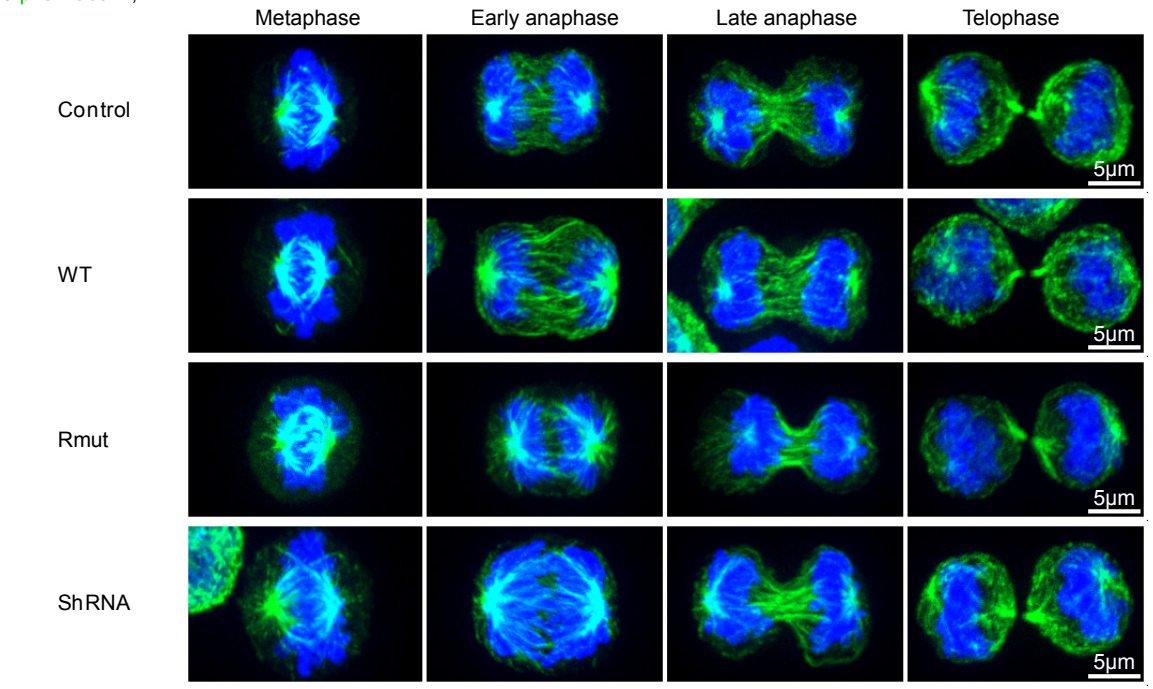

Fig. S4: Manipulation of ARHGAP19 levels or activity does not induce noticeable defects in microtubule organization in dividing lymphocytes. Kit225 lymphocytes (control, expressing the WT or Rmut forms of ARHGAP19, or depleted in ARHGAP19) were fixed using PFA. Cells were labeled for DNA (Hoechst, blue) and alpha-Tubulin (green). Representative pictures of cells in metaphase, early anaphase, mid-anaphase or telophase are shown.

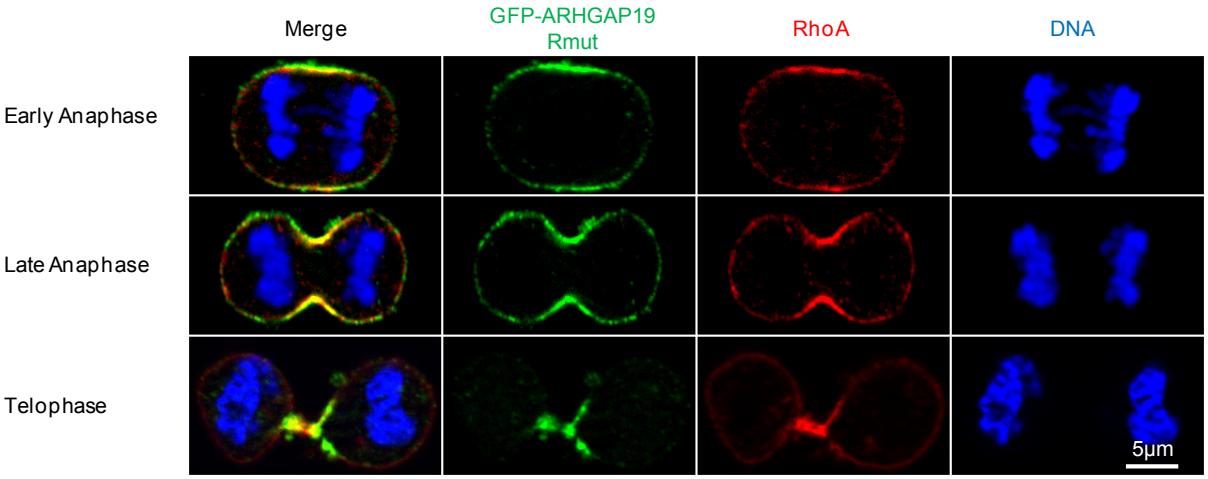

Fig. S5: GFP-ARHGAP19 Rmut and RhoA co-localize in anaphase. GFP-ARHGAP19 Rmut-expressing Kit225 lymphocytes were fixed using TCA and labeled for DNA (Hoechst, blue) and RhoA (red). GFP signals are displayed in green color. Representative pictures of mitotic cells are shown.

Movie 1. Control Kit225 lymphocyte undergoing mitosis. Mitosis progression of control Kit225 lymphocytes was followed by time lapse confocal microscopy. The red color corresponds to fluorescence emitted by the DNA labeling, Syto 59 dye. Frames were taken every minute. Selected video stills are shown in Fig. 3.

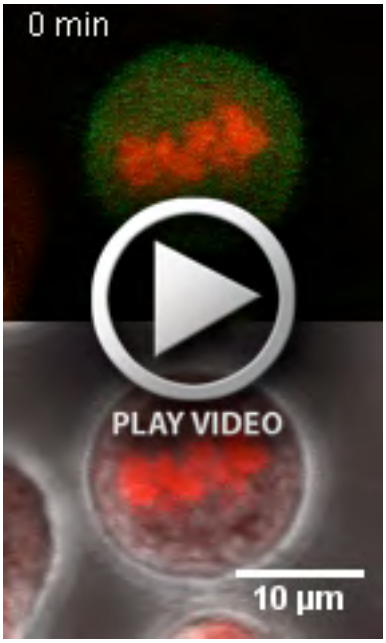

Movie 2. Mitosis of a GFP-ARHGAP19 WT-expressing Kit225 lymphocyte, with delayed cell elongation and cleavage furrow ingression as compared to control cells. Mitosis progression of Kit225 lymphocytes expressing GFP-ARHGAP19 WT (green) was followed by time lapse confocal microscopy. The red color corresponds to fluorescence emitted by the DNA labeling, Syto 59 dye. Frames were taken every minute. Selected video stills are shown in Fig. 3.

Movie 3. Examples of dividing ARHGAP19-depleted Kit225 lymphocytes: Mitosis progression of Kit225 lymphocytes transfected with ShRNA constructs targeting ARHGAP19 was followed by time lapse confocal microscopy. The red color corresponds to fluorescence emitted by the DNA labeling, Syto 59 dye. Frames were taken every minute. Selected video stills are shown in Fig. 3. The left panel shows an ARHGAP19-depleted lymphocyte that divides without major phenotype except for excessive blebbing. The middle panel illustrates the excessive cell elongation and early furrow ingression induced by silencing of *ARHGAP19*. Moderate lagging of DNA is detectable. The right panel shows a dividing ARHGAP19-depleted lymphocyte with moderate cell shape phenotype but major defects in chromosome segregation.

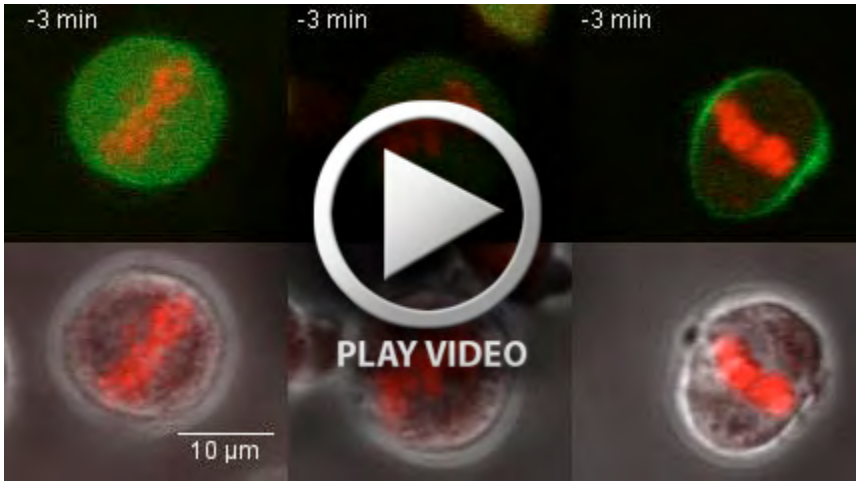

Movie 4. Examples of dividing lymphocytes expressing the R143A dominant negative form of GFP-ARHGAP19. Mitosis progression of Kit225 lymphocytes expressing GFP-ARHGAP19 Rmut (green) was followed by time lapse confocal microscopy. The red color corresponds to fluorescence emitted by the DNA labeling, Syto 59 dye. Frames were taken every minute. Selected video stills are shown in Fig. 3. The left panel shows a GFP-ARHGAP19 Rmut-expressing lymphocyte that divides without major phenotype except for excessive blebbing. The middle and right panels represent GFP-ARHGAP19 Rmut-expressing lymphocytes with moderate or severe chromosome segregation defects, respectively. On the right panel, excessive cell elongation long before anaphase onset is also observable.